Journal of Computer Science and Electrical Engineering
Print ISSN: 2663-1938
Online ISSN: 2663-1946
DOI: https://doi.org/10.61784/jcsee3121

DUAL-FAIRNESS DRIVEN 3D TRAJECTORY DESIGN AND RESOURCE ALLOCATION FOR UAV-ASSISTED ISAC SYSTEMS

LuLu Jing*, Hai Wang
College of Communication Engineering, Army Engineering University, Nanjing 210000, Jiangsu, China.
**Corresponding Author: LuLu Jing*

Abstract: Unmanned Aerial Vehicles (UAVs), recognized for their high flexibility and rapid deployment, are increasingly utilized as key platforms for Integrated Sensing and Communication (ISAC). However, balancing on-demand service quality for users with robust sensing coverage for targets remains a critical challenge, especially in emergency scenarios where blind spots must be avoided. This paper proposes a dual-fairness framework for a UAV-assisted ISCC system. We formulate a joint optimization problem of sensing, computation, communication scheduling, and UAV 3D trajectory. To ensure service fairness among users, we adopt a logarithmic utility function to maximize the sum of the logarithm of user-received data volume. Simultaneously, to guarantee sensing fairness, we enforce a Minimum Sensing Rate Ratio (MSRR) constraint, ensuring that no target is persistently neglected. The formulated non-convex problem is solved via a proposed four-stage Alternating Optimization (AO) algorithm. Simulation results demonstrate that the proposed scheme effectively balances user service fairness with sensing robustness, achieving high-quality data delivery while strictly satisfying the sensing fairness requirements.
Keywords: ISCC; UAV; Trajectory design; Logarithmic utility function; Dual-fairness

1 INTRODUCTION

Driven by emerging environment-aware applications, sixth-generation (6G) systems are evolving toward intelligent networks [1]. 6G is expected to facilitate latency-sensitive applications, including autonomous driving, telemedicine, emergency rescue, and smart industry [2]. These scenarios necessitate a tightly coupled sensing-communication-control loop [3], requiring the integration of sensing capabilities directly into the communication architecture [4]. By exploiting shared spectrum and hardware for simultaneous high-precision sensing and high-speed data transmission [5], ISAC transforms the network into a dual-functional platform capable of supporting mission-critical operations [6–8].
However, the effectiveness of ISAC critically depends on the Line-of-Sight (LoS) link between the transceiver and the target, and its performance is severely degraded by LoS obstacles. To practically deploy and optimize ISAC in dynamic and complex environments, flexible and reconfigurable network platforms are essential. In this con-text, among the various architectures that leverage ISAC, UAV-assisted wireless networks have emerged as a particularly promising solution for enabling such mission-critical applications [9]. Integrating ISAC equipment into UAVs not only conserves spectrum re-sources, but also enables simultaneous environmental sensing and communication services to ground users [10]. Capitalizing on their aerial nature, UAVs exhibit excel-lent maneuverability, featuring extended LoS propagation, wide coverage, and flexible deployment [11]. Therefore, integrating UAVs with ISAC technology can significantly enhance the system's overall sensing and communication performance [12].
The prior researches on UAV assisted ISAC systems primarily focuses on the optimal resource allocation between radar sensing and communication. In [13], Chen et al. proposed a joint sensing communication (JSC) UAV network utilizing a beam sharing scheme with orthogonal sensing and communication beams. They further developed the upper-bound average cooperative sensing area (UB-ACSA) metric to evaluate the cooperative sensing performance, and the optimal UB-ACSA was achieved by optimizing the beam sharing with specialized antennas. Zhao et al. optimized joint beamforming for ISAC systems subject to signal-dependent interference [14]. Their analysis, covering both perfect and imperfect channel state information, quantified the intrinsic trade-off between radar and communication performance. Lyu et al. studied a UAV-enabled ISAC system with a dual-functional UAV access point equipped with a vertically placed uniform linear array [15]. The UAV serves multiple users and simultaneously senses ground targets in both quasi-stationary and fully mobile scenarios. They jointly optimize the UAV maneuver and transmit beamforming to maximize the weighted sum-rate under sensing beampattern gain constraints. Wang et al. investigated the network utility maximization problem in a dual-functional radar-communication multi-UAV network [16]. By formulating a joint optimization of UAV location, user association, and transmit power under localization accuracy constraints, they proposed a decomposed iterative algorithm utilizing spectral clustering, coalition games, and successive convex approximation to effectively balance sensing and communication performance. In [17], the authors investigated a cooperative detection system utilizing multi-unmanned aerial vehicles enabled by joint radar and communication technology. They proposed a multi-agent learning-based algorithm to jointly optimize transmit power, resource allocation, and flight trajectories, effectively enhancing both sensing and data transmission performance. Meng et al. investigated an integrated sensing and communication system enabled by unmanned aerial vehicles with a periodic sensing mechanism [18]. By jointly optimizing the flight trajectory, transmit precoder, and sensing schedule, they maximized the achievable user rate under beam pattern constraints, achieving a flexible trade-off between sensing and

communication performance. Liu et al. proposed a UAV-assisted ISAC system for IoT applications [19], aiming to maximize communication throughput while explicitly accounting for the mutual interference between sensing and communication. To achieve this, they jointly optimized task scheduling, transmit power allocation, and 3D flight parameters.

Existing studies mainly focus on improving UAV-assisted ISAC systems by optimizing various performance metrics. However, they typically overlook the real-time processing requirement of sensed data and do not treat computing resources as a key dimension in system modeling and joint design. As IoT applications increasingly de-mand closed-loop "sense–compute–communicate" real-time intelligence, relying on ISAC alone is often insufficient to support timely analysis and decision-making throughout the end-to-end pipeline. Therefore, integrating computing capability deeply into the sensing and communication processes—namely, the integrated sensing, computing, and communication (ISCC) paradigm—is becoming an important evolution direction for UAV-enabled IoT networks.

Motivated by the need to fully exploit UAV mobility for mission-critical intelligence services, we investigate a single-UAV ISCC system, where a 3D mobile UAV dynamically alternates between radar sensing, onboard computation, and downlink communication to monitor multiple ground targets, process the sensed data, and de-liver the resulting intelligence to multiple users. We propose a single-UAV enabled ISCC model that integrates sensing–computing–communication in orthogonal time slots. In each sensing slot, the UAV allocates time between radar sensing and onboard computing, and then transmits the processed intelligence in downlink communication slots. To ensure dual-domain fairness, we introduce the Minimum Sensing Rate Ratio (MSRR) to guarantee equitable sensing coverage across all targets, and adopt a logarithmic utility of user-received data volume to characterize fair end-to-end service among users. The joint optimization of scheduling, time allocation, UAV frequency, power, and 3D trajectory yields a non-convex MINLP due to binary decisions and coupled non-convex rate/energy expressions. Based on this reformulation, we propose an efficient four-block alternating optimization (AO) algorithm, which decomposes the problem into tractable subproblems for (i) scheduling, (ii) sensing-and-computing time allocation and operating frequency optimization, (iii) transmit power control, and (iv) 3D trajectory optimization. Each subproblem is solved efficiently via convex optimization (and mixed-integer programming for scheduling), where the successive convex approximation (SCA) technique is employed to handle the remaining non-convex components. The resulting algorithm monotonically improves the objective value and converges to a stationary solution.

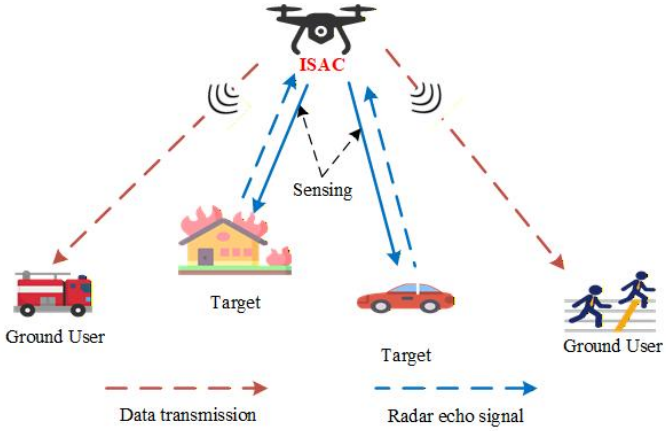

Figure 1 Proposed UAV Assisted ISAC System Model

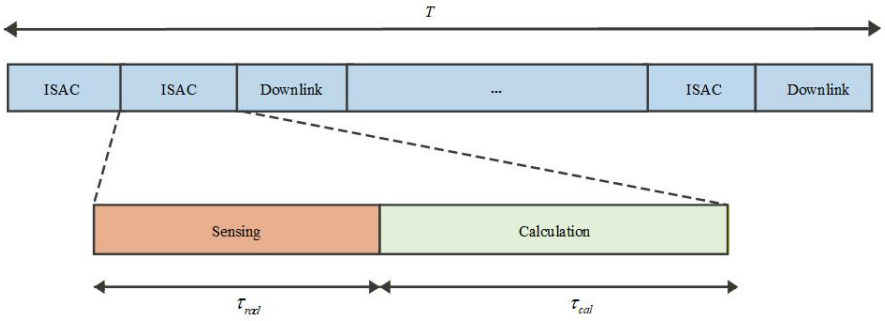

Figure 2 Slot's Structure

2 SYSTEM MODEL AND PROBLEM FORMULATION

2.1 UAV Motion and Scheduling Model

As illustrated in Figure 1, we consider a single UAV-assisted ISAC system consisting of K sensing targets and M ground users. The target and user sets are denoted by $k \in \mathcal{K} = \{1, 2, \cdots, K\}$ and $m \in \mathcal{M} = \{1, 2, \cdots, M\}$, respectively.

The total flight period T is discretized into N equal time slots, indexed by $n \in \mathcal{N} = \{1,2,\cdots,N\}$. The slot duration is $\delta = T/N$. Let $\mathbf{g}_k = (x_k, y_k)$ and $\mathbf{g}_m = (x_m, y_m)$ denote the horizontal coordinates of target k and user m, respectively. The UAV is equipped with an ISAC transceiver and flies at a time varying altitude. At slot $n \in \mathcal{N}$, the UAV's 3D position is represented by $(\mathbf{q}[n], H_u[n])$, where $\mathbf{q}[n] = (x_u, y_u)$ denotes its horizontal coordinates and $H_u[n]$ denotes its altitude. Specifically, each time slot is exclusively scheduled for either radar sensing or data downlink. As shown in Figure 2, a sensing slot δ is further divided into a sensing sub-phase τ_{rad} and computation sub-phase τ_{cal}. Specifically, the duration of the sensing sub-slot and computation sub-slot are $\tau_{rad}[n] = \varepsilon[n]\delta$ and $\tau_{cal}[n] = (1-\varepsilon[n])\delta$, respectively, where $\varepsilon[n]$ is a variable distribution coefficient. Accordingly, the time allocation must satisfy the constraint $0 \le \varepsilon[n] \le 1, \forall n$. The UAV's trajectory is strictly constrained by its physical maneuverability. Let $\mathbf{v}[n] = (v_{xy}[n], v_z[n])^T$ and $\mathbf{a}[n] = (a_{xy}[n], a_z[n])^T$ denote the UAV's velocity and acceleration in time slot n, respectively. Based on the discrete-time kinematic model, the UAV's state updates are governed by the following equations:

$$\mathbf{v}[n+1] = \mathbf{v}[n] + \mathbf{a}[n]\delta, \forall n \tag{1}$$

$$H_u[n+1] = H_u[n] + v_z[n]\delta, \forall n \tag{2}$$

$$\mathbf{q}[n+1] = \mathbf{q}[n] + v_{xy}[n]\delta, \forall n \tag{3}$$

$$V_{\min} \le \|\mathbf{v}[n]\| \le V_{\max}, \forall n \tag{4}$$

$$\|a_{xy}\| \le a_{xy}^{\max}, \|a_z[n]\| \le a_z^{\max}, \forall n \tag{5}$$

where $V_{\min}, V_{\max}$ and $a_{xy}^{\max}, a_z^{\max}$ denote the speed and acceleration limits. Additionally, to ensure flight safety and reliable communication, the UAV's altitude is restricted within a safe operational range:

$$H_{\min} \le H_u[n] \le H_{\max} \tag{6}$$

where $H_{\min}$ and $H_{\max}$ represent the minimum and maximum allowable altitudes, respectively. Finally, the initial and final states are constrained as:

$$\mathbf{q}[N] = \mathbf{q}[1], H_u[N] = H_u[1] \tag{7}$$

To mathematically characterize the time-domain task scheduling, we introduce two binary optimization variables. Let $\alpha_m[n] \in \{0,1\}$ and $\omega_k[n] \in \{0,1\}$ indicate the scheduling status of radar sensing for target k and data downlink to user m in time slot n, respectively. Specifically, $\omega_k[n] = 1$ denotes that slot n is dedicated to sensing target k, while $\alpha_m[n] = 1$ denotes that it is assigned for data transmission to user m. The scheduling variables must satisfy the following exclusivity constraint:

$$\sum_{k=1}^{K} \omega_k[n] + \sum_{m=1}^{M} \alpha_m[n] \le 1, \forall n \tag{8}$$

2.2 UAV Sensing Model

Due to the UAV's high operational altitude, we assume that the Air-to-Ground (A2G) links are dominated by Line-of-Sight (LoS) propagation. Consequently, the channel variations are mainly determined by the free-space path loss. The Euclidean distances from the UAV to the target k in slot n are calculated as:

$$d_k^2[n] = \|\mathbf{q}[n] - \mathbf{g}_k\|^2 + (H_u[n] - H_k)^2 \tag{9}$$

The channel power gain of the radar sensing link between UAV to the target k in slot n can be expressed as:

$$h_{u,k}^r[n] = \frac{\beta_r}{d_k^2[n]} = \frac{G_t G_r \lambda^2 \sigma}{(4\pi)^3 d_k^4[n]}, \forall k, n \tag{10}$$

where G_t and G_r is the antenna gain of UAV radar transmitter and receiver, σ represents the radar cross-section (RCS) of the target, $\lambda = c/f_0$ is the carrier wavelength determined by the speed of light c and carrier frequency f_0 and $\beta_r = G_t G_r \lambda^2 \sigma / (4\pi)^3$. Let $P[n]$ denote the UAV transmit power in time slot n, which needs to satisfy the following constraint:

$$0 \le P[n] \le P_{\max}, \forall n \tag{11}$$

where $P_{\max}$ represents the maximum allowable transmit power. The signal-to interference-plus-noise ratio (SINR) of the sensing link is given by

$$\Gamma_{u,k}^{r}[n]=\frac{P[n]h_{u,k}^{r}[n]}{N_0},\forall k,n \tag{12}$$

where N_0 is the total additive white Gaussian noise (AWGN) power.

To quantify the sensing performance from an information-theoretic perspective, we adopt the radar Mutual Information (MI) as the performance metric [18]. The MI measures the amount of information about the target's state contained in the received echo signal, representing the reduction in uncertainty regarding the target's state. Accordingly, the amount of radar MI between UAV and the target k in slot n is given by

$$R_{k,rad}[n]=\log_2\left(1+\Gamma_{u,k}^{r}[n]\right),\forall k,n \tag{13}$$

Then, we can get the sum of the radar MI for target k :

$$R_{k,rad}=\sum_{n=1}^{N}\omega_k[n]\varepsilon[n]\delta\log_2\left(1+\Gamma_{u,k}^{r}[n]\right),\forall k,n \tag{14}$$

To ensure reliable sensing, the radar MI for each target k must satisfy a minimum threshold constraint:

$$R_{k,rad}\geq\phi_{\min}\sum_{n=1}^{N}\omega_k[n],\forall k,n \tag{15}$$

where $\phi_{\min}$ denotes the minimum detection threshold.

2.3 UAV Computation Model

According to [18], the frequency of the central processing unit (CPU) should satisfy

$$0\leq f_c[n]\leq f_{\max},\forall n \tag{16}$$

where $f_{\max}$ is a maximum operating frequency limit.

To characterize the onboard processing, let C denote the number of CPU cycles required to process one bit of sensing data. To guarantee the integrity of onboard processing and prevent data backlog, the UAV's computation capacity allocated in each time slot must be sufficient to handle all the sensing data. This constraint is formulated as:

$$\frac{\left(1-\varepsilon[n]\right)\delta f_c[n]}{C}\geq\varepsilon[n]\delta BR_{k,rad}[n],\forall k,n \tag{17}$$

Furthermore, let $D_{k,rad}[n]$ represent the compressed data stream generated after the computation process. Then, the amount of computed data for target k at slot n can be expressed as:

$$D_{k,rad}[n]=\eta\varepsilon[n]\delta BR_{k,rad}[n] \tag{18}$$

where $\eta\in(0,1)$ denotes the data compression ratio.

2.4 UAV Communication Model

In the communication slot, the UAV transmits the processed data to the ground users via the downlink channel. The channel power gain of the data downlink from the UAV to user m in slot n can be modeled as:

$$h_{u,m}^{c}[n]=\frac{\beta_c}{d_m^2[n]}=\frac{G_tG_c\lambda^2}{(4\pi)^2d_m^2[n]},\forall k,n \tag{19}$$

where β_c represents the channel power gain at the reference distance of $d_k=1\mathrm{m}$. This reference gain is defined as $\beta_c=G_tG_c\lambda^2/(4\pi)^2$, where G_c represents the receiving antenna gain of the ground user, $d_m[n]$ represents the distance from the UAV to the user m in slot n which can be calculated as:

$$d_m^2[n]=\left\|\mathbf{q}[n]-\mathbf{g}_m\right\|^2+\left(H_u[n]-H_m\right)^2 \tag{20}$$

Accordingly, the SINR of the downlink is expressed as

$$\Gamma_{u,m}^{c}[n]=\frac{P_u[n]h_{u,m}^{c}[n]}{N_0},\forall m,n \tag{21}$$

Consequently, the achievable communication rate for user m in slot n is formulated as:

$$R_{m,com}[n]=\log_2\left(1+\Gamma_{u,m}^{c}[n]\right),\forall m,n \tag{22}$$

To guarantee the complete transmission of the computation results to the user, the downlink communication capacity must be strictly larger than the size of the computed data. This constraint is expressed as:

$$\sum_{t=1}^{n}\alpha_m[n]\delta R_{m,com}[n]\leq\sum_{t=1}^{n}\sum_{k=1}^{K}\eta\omega_k[n]\varepsilon[n]\delta R_{k,rad}[n],\forall m \tag{23}$$

2.5 Minimum Sensing Rate Ratio Model

In the considered ISAC system, the sensing data collected from distinct ground targets contributes equally to the comprehensive situational awareness. This data criticality is particularly pronounced in emergency rescue scenarios, where ignoring any single node is unacceptable. To prevent sensing starvation and ensure equitable coverage, we incorporate a fairness mechanism based on the Minimum Sensing Rate Ratio (MSRR), reformulated specifically for the sensing task. The constraint is established as

$$\min_{k} \sum_{n=1}^{N} \omega_k[n] R_{k,rad}[n] \geq \frac{\varphi}{K} \sum_{k=1}^{K} \sum_{n=1}^{N} \omega_k[n] R_{k,rad}[n] \tag{24}$$

where φ is a fairness-control parameter. The proposed MSRR mechanism provides flexible adaptability to diverse operational requirements. The parameter $\varphi \in [0,1]$ serves as a tunable factor to regulate the strictness of the fairness requirement. Specifically, setting $\varphi = 1$ enforces absolute fairness, requiring identical sensing performance across all targets. Conversely, a smaller φ relaxes this constraint, which is suitable for delay-tolerant scenarios(e.g., environmental monitoring) where data redundancy exists. However, for the mission-critical emergency rescue scenarios considered herein, a larger value of φ is imperative. This ensures that every ground target receives adequate sensing resources, preventing critical information loss.

2.6 Minimum Sensing Rate Ratio Model

To facilitate energy-efficient resource allocation under limited battery capacity, we formulate a comprehensive energy consumption model for the UAV. We consider a fixed-wing UAV equipped with ISAC and computing capabilities. The total energy expenditure is composed of propulsion energy and task execution energy (consumed by sensing, computation, and communication). Adopting the theoretical model established in [19], the cumulative propulsion and task energies in time slot n are expressed as:

$$E_s[n] = \varepsilon[n] \delta P_u[n] \tag{25}$$

$$E_c[n] = \delta(1-\varepsilon[n]) \kappa f_c^3[n] \tag{26}$$

$$E_t[n] = \delta P_u[n] \tag{27}$$

$$E_f[n] = \delta \left(c_1 \left\| \mathbf{v}[n] \right\|^3 + \frac{c_2}{\left\| \mathbf{v}[n] \right\|} \left(1 + \frac{\left\| \mathbf{a}[n] \right\|^2}{g^2} \right) \right) \tag{28}$$

where c_1 and c_2 capture effects of the UAV hardware and flight environment, κ is the effective switched capacitance coefficient of the processor, which depends on the chip architecture, and g denotes gravitational acceleration, treated as a constant. Considering the limited onboard energy capacity, the total energy consumption of the UAV over the flight period T must be strictly bounded by a maximum energy threshold E_{all} i.e.,

$$E_{total} = \sum_{n=1}^{N} \left(E_f[n] + \left(\sum_{k=1}^{K} \omega_k[n] \right) \left(E_s[n] + E_c[n] \right) + \left(\sum_{m=1}^{M} \alpha_m[n] \right) E_t[n] \right) \leq E_{all} \tag{29}$$

where $E_s[n]$, $E_c[n]$, $E_t[n]$ and $E_f[n]$ denote the sensing, computation, communication and propulsion energies in time slot n, respectively.

2.7 Problem Formulation

In the considered energy-constrained UAV-assisted ISAC framework, the UAV is dispatched to periodically fly over designated targets to perform sensing tasks and offload the computation results to ground users. Given the finite onboard energy, we propose a dual-fairness resource allocation scheme to ensure equity in both the sensing and communication domains.

Specifically, to guarantee sensing fairness among targets, we impose the Minimum Sensing Rate Ratio (MSRR) as a hard constraint to prevent sensing starvation. Simultaneously, to achieve service fairness among users, we adopt the sum-logarithmic utility function of the effective data throughput as the optimization objective. To this end, we formulate a joint optimization problem that integrates trajectory design $\mathbf{Q} = \{\mathbf{q}[n], H_u[n], \mathbf{v}[n], \mathbf{a}[n], \forall n\}$, task scheduling $\mathbf{S} = \{\omega_k[n], \alpha_m[n], \forall n, k\}$, UAV operating frequency $\mathbf{F} = \{f_c[n], \forall n\}$, time slot Optimization $\mathbf{T} = \{\varepsilon[n], \forall n\}$ and power allocation $\mathbf{P} = \{P_u[n], \forall n\}$ expressed as:

$$\max_{\mathbf{S,T,P,F,Q}} \sum_{m=1}^{M} \ln \left(\sum_{n=1}^{N} \alpha_m[n] \delta R_{m,com}[n] \right) \tag{30}$$

$$\text{s.t.} \quad (1-8), (11), (15), (16), (17), (23), (24), (29) \tag{30a}$$

The problem (30) jointly determines the TDMA scheduling $\mathbf{S}$, the time slot allocation $\mathbf{T}=\{\varepsilon[n],\forall n\}$,the power $\mathbf{P}$, CPU-frequency $\mathbf{F}$ and the 3D UAV motion $\mathbf{Q}$. The term $\sum_{m=1}^{M}\ln\left(\sum_{n=1}^{N}\alpha_m[n]\delta R_{m,com}[n]\right)$ is used to balance user services in terms of delivered data volume, while the MSRR constraint ensures that all targets receive a fair share of sensing resources. The difficulty of (30) stems from the binary scheduling variables and the non-convex rate terms coupled with distance and propulsion-energy functions, which makes the overall formulation a mixed-integer non-convex program.

3 SOLUTION ALOGORITHM

In this section, we decompose (30) into four subproblems and convexify each of them. We then solve these convexified subproblems iteratively by updating the coupled variables. The procedure returns an approximately optimal solution to the original problem and terminates when the objective converges or the maximum number of iterations is reached. To facilitate the solving process and address the non-convexity inherent in the composite objective function, we introduce a set of auxiliary variables μ_m, where μ_m represents the lower bound of the effective data volume received by user m. Consequently, the original problem can be equivalently reformulated as:

$$\max_{\mathbf{S,T,P,F,Q}}\sum_{m=1}^{M}\ln\mu_m \tag{31}$$

$$\text{s.t.}\quad (1-8),(11),(15),(16),(17),(23),(24),(29) \tag{31a}$$

$$\mu_m\le\sum_{n=1}^{N}\alpha_m[n]\,\delta R_{m,com}[n] \tag{31a}$$

3.1 UAV Scheduling Optimization

Given fixed $\mathbf{T}$, $\mathbf{P}$, $\mathbf{F}$ and $\mathbf{Q}$, the UAV scheduling optimization problem is given as

$$\max_{\mathbf{S}}\sum_{m=1}^{M}\ln\mu_m \tag{32}$$

$$\text{s.t.}\quad (8),(15),(17),(23),(24),(29) \tag{32a}$$

$$\mu_m\le\sum_{n=1}^{N}\alpha_m[n]\,\delta R_{m,com}[n] \tag{32b}$$

$$\omega_k[n]\in[0,1],\alpha_m[n]\in[0,1],\forall n \tag{32c}$$

which is a standard Mixed-Integer Convex Programming (MICP) problem, and can be solved directly by Gurobi.

3.2 UAV Transmit Power Optimization

With the fixed $\mathbf{S}$, $\mathbf{F}$ and $\mathbf{Q}$, the UAV power optimization problem is given as

$$\max_{\mathbf{S,T,P,F,Q}}\sum_{m=1}^{M}\ln\mu_m \tag{33}$$

$$\text{s.t.}\quad (11),(15),(17),(23),(24),(29) \tag{33a}$$

$$\mu_m\le\sum_{n=1}^{N}\alpha_m[n]\,\delta R_{m,com}[n] \tag{33a}$$

Optimization problem (33) is non-convex due to the concave communication rate on the left-hand side of constraint (24) and the concave sensing rate on the right-hand side of constraint (24). To address this non-convexity, we employ the first-order Taylor expansion to approximate these two specific terms, respectively. Specifically, let $P^{(i)}[n]$ denote the optimal transmit power obtained in the i iteration. Since any concave function is globally upper-bounded by its first-order Taylor expansion, we can approximate the communication rate $R_{m,com}[n]$ in (23) and the sensing rate $R_{k,rad}[n]$ in (24) using their respective linear upper bounds at the local point $P^{(i)}[n]$.For the communication rate in constraint (33e), the linear approximation is given by:

$$R_{m,com}[n]\le R^{up}_{m,com}[n]\triangleq R^{(i)}_{m,com}[n]+\nabla_p R^{(i)}_{m,com}[n]\left(P[n]-P^{(i)}[n]\right) \tag{34}$$

$$\nabla_p R^{(i)}_{m,com}[n]=\frac{1}{\ln 2}\frac{h^c_{u,m}[n]}{N_0BP^{(i)}[n]h^c_{u,m}[n]} \tag{35}$$

$$R^{(i)}_{m,com}[n]=\log_2\left(1+\frac{P^{(i)}[n]h^c_{u,m}[n]}{N_0B}\right),\forall m,n \tag{36}$$

Similarly, for the sensing rate in constraint (24), we apply the first-order Taylor expansion to the concave term on the right-hand side:

$$R_{k,rad}[n]\le R^{up}_{k,rad}[n]\triangleq R^{(i)}_{k,rad}[n]+\nabla_p R_{k,rad}\left(P^{(i)}[n]\right)\left(P[n]-P^{(i)}[n]\right) \tag{37}$$

$$\nabla_p R_{k,rad}^{(i)}[n] = \frac{1}{\ln 2} \frac{h_{u,k}^r[n]}{N_0 B P^{(i)}[n] h_{u,k}^r[n]} \tag{38}$$

$$R_{k,rad}^{(i)}[n] = \log_2\left(1 + \frac{P^{(i)}[n] h_{u,k}^r[n]}{N_0 B}\right), \forall k, n \tag{39}$$

By substituting these linear upper bounds into the original non-convex constraints (23) and (24), we obtain the approximated convex constraints as follows:

$$\sum_{t=1}^{n} \alpha_m[n] \delta R_{m,com}^{up}[n] \le \sum_{t=1}^{n} \sum_{k=1}^{K} \eta \omega_k[n] \varepsilon \delta R_{k,rad}[n], \forall m \tag{40}$$

$$\sum_{n=1}^{N} \omega_k[n] R_{k,rad}[n] \ge \frac{\varphi}{K} \sum_{k=1}^{K} \sum_{n=1}^{N} \omega_k[n] R_{k,rad}^{up}[n], \forall k \tag{41}$$

Therefore, Problem (33) can be remodeled as:

$$\max_{\mathbf{S,T,P,F,Q}} \sum_{m=1}^{M} \ln \mu_m \tag{42}$$

$$\text{s.t.} \quad (11),(15),(17),(29),(40),(41) \tag{42a}$$

$$\mu_m \le \sum_{n=1}^{N} \alpha_m[n] \delta R_{m,com}[n] \tag{42a}$$

After the SCA transformation, subproblem (33) becomes a standard convex optimization problem. Since it involves linear and logarithmic constraints, it can be efficiently solved by interior-point methods using standard solvers such as CVX.

3.3 UAV Computation Resource Optimization

In this subproblem, we jointly optimize the time allocation variable **T** and operating frequency **F** while keeping the scheduling **S** ,transmit power **P** and trajectory **Q** fixed . The problem is given as

$$\max_{\mathbf{T,F}} \sum_{m=1}^{M} \ln \mu_m \tag{43}$$

$$\text{s.t.} \quad (15-17),(23),(24),(29) \tag{43a}$$

$$\mu_m \le \sum_{n=1}^{N} \alpha_m[n] \delta R_{m,com}[n] \tag{43b}$$

For fixed **S** , **P** and **Q** , $\sum_{m=1}^{M} \ln \mu_m$ in the objective function is a constant. To address the non-convexity caused by the coupled term $(1-\varepsilon[n]) f_c^3[n]$ in the E_{total} , we introduce an auxiliary variable. Let $\upsilon[n] = (1-\varepsilon[n]) f_c[n]$ defined as the effective computation cycles. Consequently, the original computation energy term can be reformulated as:

$$f_c[n] = \frac{\upsilon[n]}{1-\varepsilon[n]}, \forall k, n \tag{44}$$

$$\hat{E}_c[n] = \kappa\delta(1-\varepsilon[n]) f_c^3[n] = \kappa\delta(1-\varepsilon[n]) \left(\frac{\upsilon[n]}{1-\varepsilon[n]}\right)^3 = \kappa\delta \frac{(\upsilon[n])^3}{(1-\varepsilon[n])^2} \tag{45}$$

$$\hat{E}_{total} \ge \sum_{n=1}^{N} \left(E_f[n] + \left(\sum_{k=1}^{K} \omega_k[n]\right) \left(E_s[n] + \kappa\delta \frac{(\upsilon[n])^3}{(1-\varepsilon[n])^2} \right) + \left(\sum_{m=1}^{M} \alpha_m[n]\right) E_t[n] \right) \tag{46}$$

where the transformed term $\frac{(\upsilon[n])^3}{(1-\varepsilon[n])^2}$ can be identified as the perspective function. In order to solve problem (43), we need to use linear substitution functions to replace E_{total} , which can be written as (46). Therefore, the optimization problem (43) can be reformulated as

$$\max_{\{\upsilon[n],\varepsilon[n]\}} \left\{ \sum_{m=1}^{M} \ln \mu_m + \vartheta \hat{E}_{total} \right\} \tag{47}$$

$$\text{s.t.} \quad (15-17),(44-46) \tag{47a}$$

$$\mu_m \le \sum_{n=1}^{N} \alpha_m[n] \delta R_{m,com}[n] \tag{47b}$$

which is convex and can be solved by the CVX, ϑ is a negative coefficient.

3.4 UAV 3D Trajectory Optimization

In this subproblem, we optimize the UAV 3D trajectory **Q** with fixed resource allocation **F** , **S** **P** , **T** . The problem is formulated as:

$$\max_{\mathbf{Q}} \sum_{m=1}^{M} \ln \mu_m \tag{48}$$

$$\text{s.t.} \quad (1-8),(11),(15),(16),(17),(23),(24),(29) \tag{48a}$$

$$\mu_m \le \sum_{n=1}^{N} \alpha_m[n]\, \delta R_{m,com}[n] \tag{48b}$$

We can see that problem (48) is non-convex due to the non-convex objective function and constraints involving the UAV location variables in the rate terms. To tackle this, we employ the SCA technique. By (19)-(22) and (10)-(14), we can obtain,

$$R_{m,com}[n] = \log_2\left(1+\frac{P[n]h_{u,m}^{c}[n]}{N_0 B}\right) = \frac{1}{In2} In\left(1+\frac{P[n]\beta_c}{N_0 B d_m^2[n]}\right) \tag{49}$$

$$R_{k,rad}[n] = \log_2\left(1+\frac{P[n]h_{u,k}^{r}[n]}{N_0 B}\right) = \frac{1}{In2} In\left(1+\frac{P[n]\beta_r}{N_0 B d_k^4[n]}\right) \tag{50}$$

Specifically, (49) - (50) are lower-bounded by their first-order Taylor approximations constructed at the point $d_m^2[n] = \left\|\mathbf{q}^{(i)}[n]-\mathbf{g}_m\right\|^2 + H_u^{2(i)}[n]$ and $d_k^{2(i)} = \left\|\mathbf{q}^{(i)}[n]-\mathbf{g}_k\right\|^2 + H_u^{2(i)}[n]$. For the communication rate in (48), the linear approximation is reformulated as:

$$R_{m,com}[n] \ge R_{m,com}^{lb}[n] \triangleq \frac{1}{In2} In\left(1+\frac{P[n]\beta_c}{N_0 B d_m^{2(i)}[n]}\right) + \nabla_{d_m^2[n]} R_{m,com}^{(i)}[n]\left(d_m^2[n]-d_m^{2(i)}[n]\right) \tag{51}$$

$$\nabla_{d_m^2[n]} R_{m,com}^{(i)}[n] = -\frac{1}{In2}\frac{P_u[n]\beta_c}{\left(P_u[n]\beta_c + N_0 B d_m^{2(i)}\right) d_m^{2(i)}} \tag{52}$$

Similarly, for the sensing rate

$$R_{k,rad}[n] \ge R_{k,rad}^{lb}[n] \triangleq \frac{1}{In2} In\left(1+\frac{P[n]\beta_r}{N_0 B d_k^{4(i)}[n]}\right) + \nabla_{d_k^{2(j)}} R_{k,rad}[n]\left(d_k^2[n]-d_k^{2(j)}[n]\right) \tag{53}$$

$$\nabla_{d_k^2[n]} R_{k,rad}^{(i)}[n] = \frac{2}{In2}\frac{-P[n]\beta_r}{\left(P[n]\beta_r + N_0 B d_k^{4(i)}\right) d_k^{2(i)}} \tag{54}$$

Since $d_m^2[n]-d_m^{2(i)}[n]$ and $d_k^2[n]-d_k^{2(j)}[n]$ are convex function, the auxiliary variable is introduced to further relax:

$$\chi_m[n] \ge d_m^2[n]-d_m^{2(i)}[n] = \left(\left\|\mathbf{q}[n]-\mathbf{g}_m\right\|^2 + H_u^2[n]\right) - \left(\left\|\mathbf{q}[n]-\mathbf{g}_m\right\|^2 + H_u^{2(i)}[n]\right) \tag{55}$$

$$\chi_k[n] \ge d_k^2[n]-d_k^{2(i)}[n] = \left(\left\|\mathbf{q}[n]-\mathbf{g}_k\right\|^2 + H_u^2[n]\right) - \left(\left\|\mathbf{q}[n]-\mathbf{g}_k\right\|^2 + H_u^{2(i)}[n]\right) \tag{56}$$

For the non-convex item $E_f[n]$ and the constraint (48d), we introduce a slack variable $\chi_e^2[n] \le \left\|\mathbf{v}[n]\right\|^2$. Then $E_f[n]$ can be rewritten as

$$\tilde{E}_f = \sum_{n=1}^{N} \delta\left(c_1\left\|\mathbf{v}[n]\right\|^3 + \frac{c_2}{\left\|\chi_e[n]\right\|}\left(1+\frac{\left\|\mathbf{a}[n]\right\|^2}{g^2}\right)\right) \tag{56}$$

For any fixed point $\mathbf{v}^{(i)}[n]$, $\left\|\mathbf{v}[n]\right\|^2$ can be rewritten as

$$\left\|\mathbf{v}[n]\right\|^2 \ge \mathbf{v}^{lb}[n] = \left\|\mathbf{v}^{(i)}[n]\right\|^2 + 2\mathbf{v}^{(i)}[n]^T\left(\mathbf{v}[n]-\mathbf{v}^{(i)}[n]\right) \tag{56}$$

Based on (51)-(56), the problem (48) can be equivalently expressed as the following:

$$\max_{\mathbf{Q}} \sum_{m=1}^{M} \ln \mu_m \tag{57}$$

$$\text{s.t.} \quad (1-8) \tag{57a}$$

$$\chi_e^2[n] \le \mathbf{v}^{lb}[n], \chi_e[n] \ge V_{\min}, \forall k,n \tag{57b}$$

$$\sum_{n=1}^{N} \omega_k[n]\varepsilon[n]\delta R_{k,rad}^{lb}[n] \ge \phi_{\min}\sum_{n=1}^{N}\omega_k[n], \forall k,n \tag{57c}$$

$$\frac{\delta\left(1-\varepsilon[n]\right) f_c[n]}{C} \ge \varepsilon[n]\delta B R_{k,rad}[n], \forall k,n \tag{57d}$$

$$\sum_{t=1}^{n} \alpha_m[n]\delta R_{m,com}[n] \le \sum_{t=1}^{n}\sum_{k=1}^{K}\eta\omega_k[n]\varepsilon[n]\delta R_{k,rad}^{lb}[n], \forall m \tag{57e}$$

$$\sum_{n=1}^{N}\omega_k[n]R_{k,rad}^{lb}[n] \ge \frac{\varphi}{K}\sum_{k=1}^{K}\sum_{n=1}^{N}\omega_k[n]R_{k,rad}[n] \tag{57f}$$

$$\tilde{E}_{total} = \sum_{n=1}^{N}\left(\tilde{E}_f[n] + \left(\sum_{k=1}^{K}\omega_k[n]\right)\left(E_s[n] + E_c[n]\right) + \left(\sum_{m=1}^{M}\alpha_m[n]\right)E_t[n]\right) \le E_{all} \quad (57g)$$

which is a convex problem and can be solved through CVX.

4 SIMULATION RESULTS

We consider a UAV-enabled ISAC system operating in a 3D area of $1000m \times 1000m$. The system consists of $M = 2$ communication users and $K = 8$ sensing targets randomly distributed on the ground. The UAV is dispatched to perform a dual-functional mission that providing downlink data transmission to the users and performing radar sensing on the targets within a mission period of $T = 120s$. The specific parameter values in this paper refer to [19].

The initialization of the UAV trajectory influences the convergence behavior and the final performance. Following the initialization method in [19], we construct the initial UAV trajectory and set the initial altitude to 150 m. The 3D trajectory of the UAV is depicted in Figure 3. In this figure, the red circles represent the IoT targets, the blue squares represent users. The red dotted circle indicates the initial trajectory. The optimized trajectory of UAV is represented by gradient color, and gradient color represents the change of UAV flying height. From the figure, we can clearly see the flight direction and trajectory of the UAV. It can be observed that the UAV will try to fly over each sensing target as much as possible to obtain better channel conditions, and the altitude change is to meet the flight conditions and obtain more sensing data.

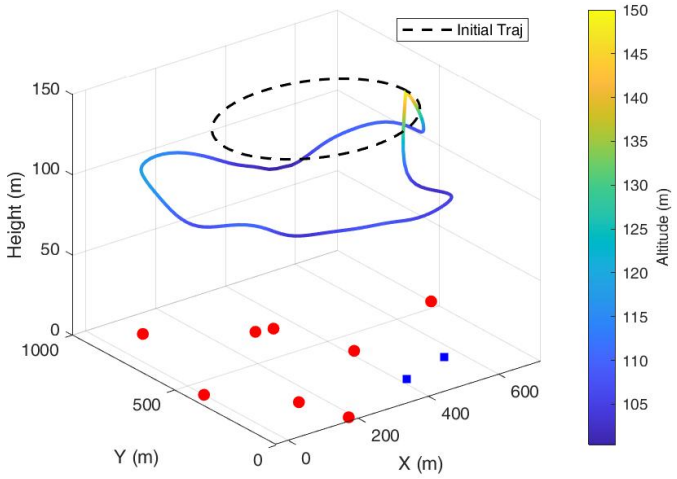

Figure 3 Initial and Converged UAV 3D Trajectories

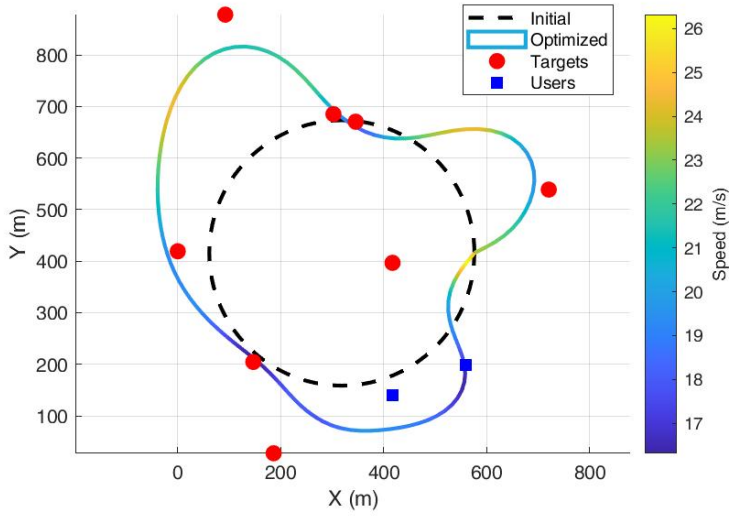

Figure 4 A Top View of the Optimized 3D Trajectories

Figure 4 shows the top view of the optimized 3D trajectory, and the gradual color indicates the flight speed of the UAV. It can be observed that the UAV will slow down to obtain more perceptual data when it is close to the target.

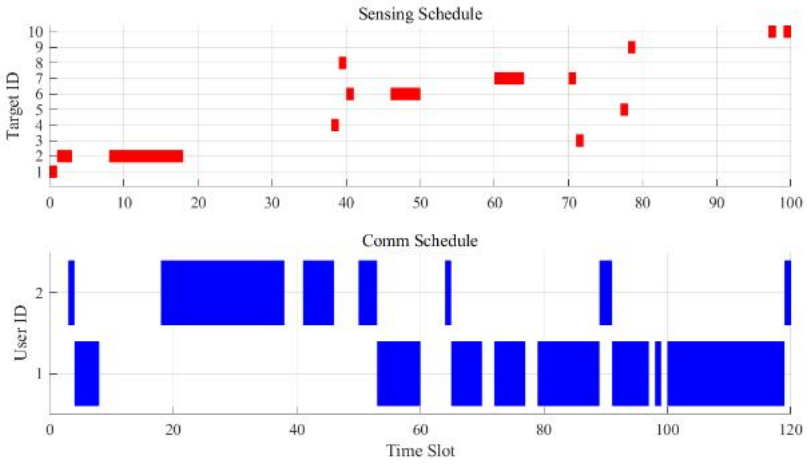

Figure 5 ISAC Scheduling of UAVs at Each Time Slot

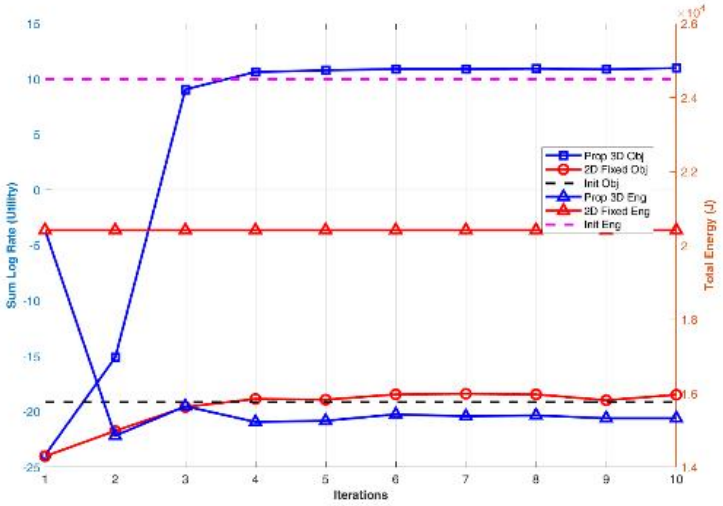

Figure 6 Comparison of Different Algorithms

Figure 5 shows the scheduling situation of nodes in each time slot and the service time slot for users. Figure 6 illustrates the convergence behavior and performance comparison of the proposed 3D trajectory optimization algorithm against the 2D fixed-height scheme ($H = 120$) and the initial trajectory benchmark. The left y-axis represents the system utility (Sum Log Rate), while the right y-axis denotes the total energy consumption.

5 CONCLUSIONS

This paper studied a single-UAV assisted ISCC system that alternates between radar sensing for multiple ground targets and data transmission to multiple users. To achieve dual fairness in an end-to-end manner, we adopted the sum-logarithmic utility of user-received data volume to characterize fair end-to-end service among users, and employed the Minimum Sensing Rate Ratio (MSRR) requirement to prevent persistent sensing starvation across targets. The resulting joint design is inherently challenging due to the coupled decision variables and the non-convex rate/energy expressions. To avoid premature termination caused by initial infeasibility, we developed a penalty-based framework that transforms key hard constraints into hinge-loss penalty terms embedded in the objective function, yielding an augmented optimization problem. Based on this reformulation, we further proposed an iterative solution based on alternating optimization (AO) and successive convex approximation (SCA), where each subproblem is solved efficiently via convex optimization. Simulation results validated that the proposed approach can effectively balance end-to-end user service fairness and target sensing fairness under practical resource constraints, and achieves stable performance improvements compared with benchmark schemes. Future work may extend the proposed penalty-based dual-fairness framework to multi-UAV cooperative ISCC scenarios.

COMPETING INTERESTS

The authors have no relevant financial or non-financial interests to disclose.

REFERENCES

[1] Nguyen D C, Ding M, Pathirana P N, et al. 6G Internet of Things: A Comprehensive Survey. IEEE Internet of Things Journal, 2022, 9(1): 359-383.
[2] Wei Z, Qu G, Fan P, et al. Integrated Sensing and Communication Signals Toward 5G-A and 6G: A Survey. IEEE Internet of Things Journal, 2023, 10(13): 11068-11092.
[3] Zhu X, Liu C, Shu F, et al. Enabling Intelligent Connectivity: A Survey of Secure ISAC in 6G Networks. IEEE Communications Surveys & Tutorials, 2025, 27(2): 748-781.
[4] Liu F, Masouros C, Petropulu A P, et al. Joint Radar and Communication Design: Applications, State-of-the-Art, and the Road Ahead. IEEE Transactions on Communications, 2020, 68(6): 3834-3862.
[5] Zhang J A, Rahman M L, Wu K, et al. An Overview of Signal Processing Techniques for Joint Communication and Radar Sensing. IEEE Journal of Selected Topics in Signal Processing, 2021, 15(6): 1295-1315.
[6] Li G, Liu B, Xu P, et al. Integrated Sensing and Communication From Learning Perspective: An SDP3 Approach. IEEE Internet of Things Journal, 2024, 11(4): 5589-5603.
[7] Dou C, Huang N, Wu Y, et al. Integrated Sensing and Communication Enabled Multidevice Multitarget Cooperative Sensing: A Fairness-Aware Design. IEEE Internet of Things Journal, 2024, 11(17): 29190-29201.
[8] Li N, Wang B, Zhu J. An Overview of Standardization Progress for Integrated Sensing and Communications: Use Cases, Channel Modeling and Potential Challenges. 2024 10th International Conference on Computer and Communications (ICCC), Chengdu, China, 2024: 2406-2411.
[9] Ahmed M, Nasir A A, Masood M, et al. Advancements in UAV-based integrated sensing and communication: A comprehensive survey. arXiv preprint arXiv:2501.06526, 2025.
[10] Mu J, Zhang R, Cui Y, et al. UAV Meets Integrated Sensing and Communication: Challenges and Future Directions. IEEE Communications Magazine, 2023, 61(5): 62-67.
[11] Rezaei O, Naghsh M M, Karbasi S M, et al. Resource Allocation for UAV-Enabled Integrated Sensing and Communication (ISAC) via Multi-Objective Optimization. ICASSP 2023 - 2023 IEEE International Conference on Acoustics, Speech and Signal Processing (ICASSP), Rhodes Island, Greece, 2023: 1-5.
[12] Zhang J A, Liu F, Masouros C, et al. Enabling Joint Communication and Radar Sensing in Mobile Networks—A Survey. IEEE Communications Surveys & Tutorials, 2022, 24(1): 306-345.
[13] Chen X, Feng Z, Wei Z, et al. Performance of Joint Sensing-Communication Cooperative Sensing UAV Network. IEEE Transactions on Vehicular Technology, 2020, 69(12): 15545-15556.
[14] Zhao N, Wang Y, Zhang Z, et al. Joint Transmit and Receive Beamforming Design for Integrated Sensing and Communication. IEEE Communications Letters, 2022, 26(3): 662-666.
[15] Lyu Z, Zhu G, Xu J. Joint Maneuver and Beamforming Design for UAV-Enabled Integrated Sensing and Communication. IEEE Transactions on Wireless Communications, 2023, 22(4): 2424-2440.
[16] Wang X, Fei Z, Zhang J A, et al. Constrained Utility Maximization in Dual-Functional Radar-Communication Multi-UAV Networks. IEEE Transactions on Communications, 2021, 69(4): 2660-2672.
[17] Zhang T, Zhu K, Zheng S, et al. Trajectory Design and Power Control for Joint Radar and Communication Enabled Multi-UAV Cooperative Detection Systems. IEEE Transactions on Communications, 2023, 71(1): 158-172.
[18] Liu Z, Liu X, Yang W, et al. Joint Sensing and Age of Information Optimization for Energy Constrained UAV-Assisted Integrated Sensing, Calculation, and Communication. IEEE Transactions on Wireless Communications, 2025, 24(5): 4440-4453.
[19] Jing L, Wang H, Qin Z, et al. Energy-Efficient 3D Trajectory Optimization and Resource Allocation for UAV-Enabled ISAC Systems. Entropy, 2026, 28(2): 248.